MTR180488
MITRE TECHNICAL REPORT

MITRE

Commercial Snapshot Spectral Imaging: The Art of the Possible

Sponsor: MITRE Innovation Program
Dept. No.: P531 & T821
Project No.: 10MSRF18-ZL

Approved for public release; Distribution unlimited. Public Release Case Number 18-3832.

Michael West
John Grossmann
Chris Galvan

September 2018

McLean, VA

This page intentionally left blank.

Abstract

Advancements in snapshot multi- and hyper-spectral technology will soon make spectral imaging available to the consumer market. The first wave of products will be dominated by visible to near infrared (VNIR) cameras due to the maturity of Charged Coupled Device (CCD)/Complementary Metal Oxide Semiconductor (CMOS) imaging chip technology, which is used in everything from cell phone cameras to the Hubble Space Telescope. There is great potential for the law enforcement, war fighter, and intelligence communities to deploy compact spectral imaging on cell phones, dash cams, and small unmanned aerial vehicles (UAVs). These uses of VNIR imaging spectroscopy go beyond the conventional ones, including agricultural and food safety applications that typically use VNIR spectroscopy. In this document we explore the "art of the possible" in VNIR imaging spectroscopy to enable material identification and characterization with low cost (i.e., non-scientific grade) commercial imagers.

This page intentionally left blank.

Executive Summary

This report summarizes a study on the state-of-the-art and anticipated advancements in commercial snapshot spectral imaging. Spectral remote sensing as a method of determining material properties had been a tool solely used by governmental organizations, universities, and corporations due to the expense of the technology. However, advancements in snapshot multi- and hyperspectral technology will soon make spectral imaging available to the consumer market.The first wave of products will be dominated by visible to near infrared (VNIR) cameras due to the maturity of Charged Coupled Device (CCD)/Complementary Metal Oxide Semiconductor (CMOS) imaging chip technology used in everything from cell phones cameras to the Hubble Space Telescope.

We performed a comprehensive review of the state-of-the-art in snapshot spectral imaging and identified exemplar devices that represent what we believe are the most promising technologies for achieving a low-cost hyperspectral imager that can either be fit on a cell phone or small form factor stand-along camera similar to a DSLR. It should be noted that there are other small size hyperspectral imagers available on the market, such as the Headwall Nano-Hyperspec[1] and Corning microHSI[2]. However,the Headwall and Corning systems are not snapshot systems; they are line-scanning cameras that require motion from a platform, such as a UAV. We identify four main categories of snapshot spectral imaging:

- Fabry-Perot micro-electromechanical system (MEMS) interferometer.
- Custom color Bayer matrix filters.
- Static Fabry-Perot color tile matrix filters.
- Line-scanner with internal scan mirror.

The first is micro-electromechanical system (MEMS) Fabry-Perot interferometer, which dynamically scans the spectral bandpass by changing the distance between two etalons while capturing individual frames to build up the data cube. The trade-off is that you obtain the full spatial resolution at the cost of increased time necessary to scan across all the wavelengths.The second and third technologies are variants of the same concept of creating customized color filters in front of the focal plane. All consumer-level color cameras have 3-color Bayer matrix with red-green-blue (RGB) filters that approximate human eye color response. One approach is to add more colors to the Bayer matrix. Another is to place static Fabry-Perot filters with specific band passes in front of the focal plane. Both methods capture all the spectral bands at once. One of the trade-offs with this approach is sacrificing spatial resolution for additional spectral bands. Though not strictly "snapshot," there are also line-scanning devices that employ moving internal parts to perform the scan

We identified six applications where we feel snapshot spectral imaging could have a significant impact.

[1] http://www.headwallphotonics.com/hyperspectral-sensors

[2] https://www.corning.com/worldwide/en/products/advanced-optics/product-materials/spectral-sensing.html

- Counter Denial & Deception (e.g., detecting camouflage)
- Search & Rescue
- First Responders
- Medicine
- Law Enforcement/Security
- Crime-scene Forensics

The applications listed above are where we see immediate benefit given the *portability* of handheld, snapshot implementation of VNIR imaging technology. We expect other applications will come to fruition when the technology becomes more widely available to the general consumer market.

The technology to create portable, snapshot hyperspectral cameras is already here (see Appendix B for a detailed list of current products.) It will only be a few years before the technology will appear in commercial devices, such as cell phone and palm-sized cameras. We have presented in this report an overview of the current state-of-the-art in VNIR spectral imaging technology with an eye towards smaller, portable devices and the potential applications of the technology provided certain technical challenges are overcome. We expect that first-adopters and the Do-it-Yourself (DIY) community will come up with applications that neither we nor the vendors have thought of, much like what happened with smart phones. There is a need to continue to monitor the technology and develop algorithms and prototype hardware to avoid technical surprise, such as foreign adversaries using the technology for clandestine collection or criminals intent on defeating security measures.

Table of Contents

List of Figures

1 Introduction

Since the early 19th-century, optical spectroscopy has been a powerful tool for identifying the chemical composition of objects from standoff distances ranging from a few millimeters to tens of thousands of light years. Spectroscopy is used to identify the elemental and molecular composition of materials by the unique "finger print" of emission and absorption features produced by atomic transitions and vibrations of bonded molecules, with the latter being the primary mechanism producing identifiable features in manmade materials. In general, the strongest features produced by the vibrational modes of molecules appear in the shortwave (0.9-2.5 micrometers) and longwave (7.5-13.5 micrometers) region of the electromagnetic spectrum. Theoretically, molecular vibrational overtones should appear in the VNIR, though they are usually very weak.

Vendors are initially marketing commercial Visible-to-Near-InfraRed (VNIR) spectral cameras primarily for agricultural[1] and food safety[2] applications. Material-identifying information in the form of absorption features mostly reside in the short-wave infrared (SWIR) to long-wave infrared (LWIR) regions of the spectrum (1.0 μm to 14.0 μm.) These absorption features arise from molecular vibrations. However, the current state of SWIR and LWIR focal plane technology makes the mass production of low-cost, consumer-grade cameras cost-prohibitive. The first wave of mass-produced spectral imaging cameras will be made with silicon CCD and CMOS focal planes such as those used in digital cameras. CCD and CMOS focal planes can be produced with millions of pixels, which translates into higher spectral and spatial resolution as compared to lower pixel density focal planes made for SWIR to LWIR cameras. Spectral cameras are already being sold and primarily used for agricultural applications.

Manufacturers are increasingly developing low-cost portable point spectrometers and multi-spectral cameras (4 or more color bands) that can be operated from cellphones. These devices are being marketed for consumer food safety and quality inspection to check for the presence of spoilage and ripeness of fruit. The technological push is to create hyperspectral imagers with 10's to 100's of color bands. Only CCD and CMOS focal planes can provide the pixel density for high-spatial/spectral resolution for hyperspectral imaging on a cellphone. The research question we will address focuses on what more can you do with the technology beyond food safety applications and what threat and/or advantage such devices could present.

This report is structured in the following manner. Section 2 and Section 3 provide a short overview of hyperspectral imaging and visible-to-near-infrared (VNIR) spectroscopy. A reader already familiar with spectroscopy and spectral imaging can skip ahead to Section 4, which describe some examples of spectral imaging technology available today. Section 5 describes applications where we believe this technology will have a large impact. Section 6 is a discussion of the technical challenges that need to be overcome to reap the full potential of this technology, followed by Summary and Conclusions.

2 Hyperspectral Imaging

Imaging spectroscopy offers the potential for material identification based on spectroscopic features unique to the material captured in the imagery at a stand-off. The spectral features are produced by electronic vibrational resonances in the visible and ultraviolet and by molecular vibrational resonances in the infrared. In the visible (VIS), near infra-red (NIR) and short wave infra-red (SWIR), the vibrational resonances are excited by active illumination such as sunlight or artificial lighting. In the long wave infra-red (LWIR), the molecular resonances are detected by self-emission or the absorption of photons emitted by sources in the background. Sensors can be designed to respond to specific ranges of wavelengths in the VIS, NIR, SWIR, or LWIR. The sensitivity of the instrument to wavelength is determined by the photo-electrical properties of the focal plane. Hyperspectral remote sensing is used in applications such as geology, vegetation science, agriculture, land use monitoring, coastal analysis, bathymetry, mine detection, law enforcement, and chemical agent detection[3].

This report will focus on silicon (Si) based focal planes because of their relative low expense and ease of manufacture. Silicon focal planes respond to wavelengths in the VIS and the NIR, called the VNIR wavelength regime (0.4μm- 1.0μm). The types of materials/gases that have spectral features in the VNIR are: atmospheric aerosols, vegetation, chlorophyll, oxygen, and iron oxides. VNIR hyperspectral imagers are not generally used to detect materials with features in the SWIR, such as geological minerals, plastics, fabrics, paints, soils, fuels, and carbon dioxide. However, it will be shown in this report that many such SWIR-specific materials can be detected under limited conditions using VNIR hyperspectral imaging because their spectra are nevertheless distinct from natural materials in the VNIR. The creation of spectral libraries for low-cost hyperspectral imagers would follow the same standard methodologies used historically. The process would be either to gather image-based signatures in the sensor units (Digital Number or DN), or in the radiance-domain after the sensor data are corrected to engineering units, or most commonly in the reflectance-domain using ground- or laboratory- based point spectrometers. Reflectance domain signatures are the most versatile as they have been corrected for illumination.

3 Basics of VNIR Spectroscopy

There are detailed descriptions of the physics behind light spectroscopy found in most physics texts and books on hyperspectral remote sensing[3] What we will cover here are the most relevant aspects of VNIR spectroscopy and how it compares to spectroscopy using other parts of the electromagnetic spectrum as exploited by hyperspectral technology. Physically, the processes that give rise to either absorption or emission spectral features are due to photon scattering, atomic-level transitions, and molecular vibrations[4].

HSI remote sensing, which was discussed in Section 2, relies heavily on spectral features produced by molecular vibrations that appear in the infrared beyond 1 μm, as shown in Figure 1. Much like a vibrating violin string, there are "overtone" features that can appear at higher frequencies, or, in this case, shorter wavelengths, that are weaker in magnitude. Therefore, it is possible to uniquely identify materials based upon VNIR-only spectroscopy.

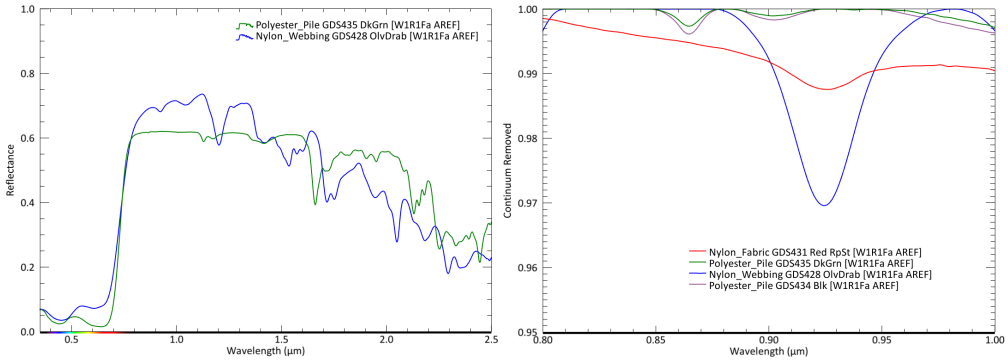

Figure 1: Examples of polyester and nylon fabrics from the USGS spectral library. The short-wave infrared region of the spectrum between 1.0μm and 2.5μm are feature-rich, making it much easier to determine material composition in the SWIR. However, there are some diagnostic features that appear in the near-infrared, though they are much weaker than in the SWIR. (Note: the figure on the right is displayed with the continuum removed to emphasize the absorption features.

Photon scattering and emissions from electronic transitions at the atomic level give rise to what humans perceive as color. For example, paint pigment formulations are all designed to produce specific colors visible to the human eye. While SWIR spectroscopy is sensitive to the chemical make-up of a substrate (e.g., fabric fiber, metal car body, etc.,) VNIR spectroscopy can uniquely identify the color pigments. There are perhaps millions of different combinations of pigments possible to produce whatever color is desired. Figure 2 shows an example of 24 colors on a Munsell color chart and the unique reflectance spectra of each square on the chart.

Photon scattering off particulate matter will produce discernable effects in reflectance spectra as a function of particle size distribution. In plain terms, there are more gaps between larger particles, which results in few photons scattering back toward an observer. Conversly, a collection of

[3] A recent and particularly good treatment of the subject can be found in Chapter 2 of Michael Eismann's book **Hyperspectral Remote Sensing**[3].

[4] There are also effects due to molecular *rotations* in gases, but we are going to limit the discussion to solids,liquids, and light sources.

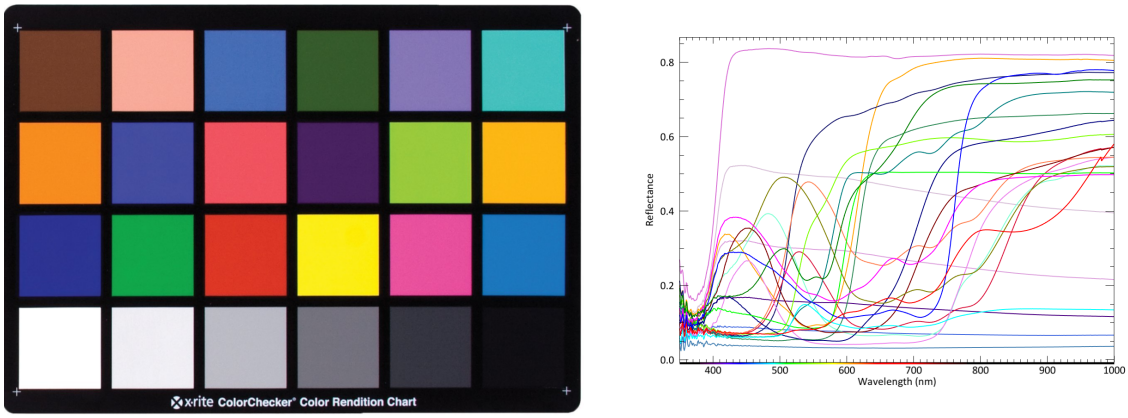

Figure 2: A standard Munsell color chart with 24 pigments display a wide variety of unique pigment signatures.

smaller/finer particles have fewer gaps between them, and thus, a higher percentage of photons scattering back toward the observer than in the large particle case. This phenomenon is observable in both the VNIR and SWIR parts of the spectrum, as shown in Figure 3. Electronic transitions give rise to coloration that uniquely identify certain mineral groups[4]. In other words, VNIR spectroscopy can and does play a role in geological analysis.

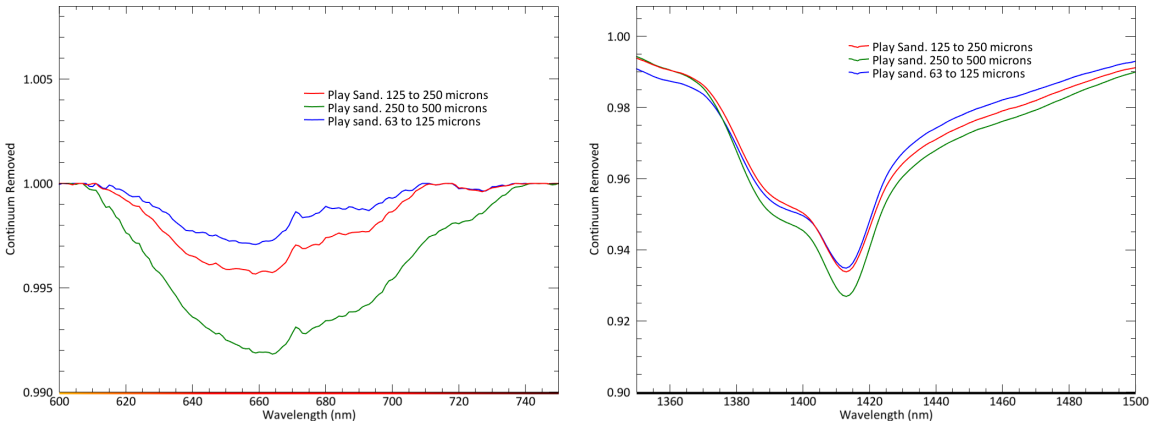

Figure 3: Reflectance spectra of quartz playsand that have been sifted into different particle size ranges. Differences in particle sizes produces effects that are discernable in both the VNIR (left) and SWIR (right) portions of the spectrum. Specifically, the absorption features become deeper as the particles sizes increase. (Note: The spectra are plotted with the continuum removed to emphasize the absorption features.)

Electronic transitions at the atomic level are responsible for light emission in the visible part of the electromagnetic spectrum. In nature, we observe these emissions from such phenomena as electrical discharges, bioluminescence, and fluorescence. There are also man-made sources, such as artificial lighting, which can can produce very distinct spectra, as shown in Figure 4. While the human eye and standard red-green-blue (RGB) color cameras can distinguish color content of lights, VNIR spectrometers can determine the specific type of light and, in some cases, the elemental composition (e.g., neon, mercury vapor, etc.)

The important take-away from this above discussion is that there is wealth of information contained

in VNIR spectra that can be exploited. The next section will discuss the current state-of-the-art in portable VNIR spectrometers, including *imaging* spectrometers.

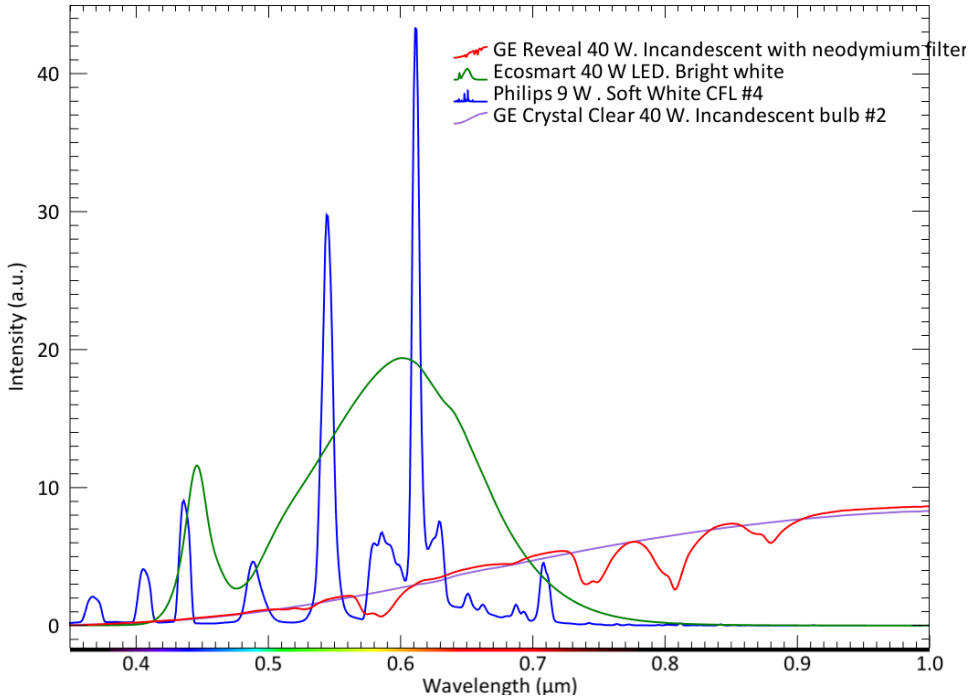

Figure 4: Emission spectra of various commercial off-the-shelf light bulbs.

4 State-of-The-Art in Snapshot Hyperspectral Imaging

A survey of published literature and industry has revealed a large number of varying types of scientific and commercial grade snapshot hyperspectral imagers available on the market. Many vendors are aimed at solving specific problems and attempting to distinguish themselves from other device manufacturers by offering a multitude of features. It can be argued that the availability of these numerous types of spectral imagers that are targeted toward specific industries is due to the fact that no one design solves all the needs of any one particular field and the spatial, spectral, and temporal requirements need to adapt to the intended application. We restrict the scope of this paper to *portable snapshot hyperspectral imaging (HSI)* and the types of devices encompassed by this definition. The references that are given have been chosen to represent the current state-of-the-art. (An exhastive list of vendors and their products can be found in Appendix B.)

To fully understand the underlying functionality of a snapshot hyperspectral imager, some background information is provided. There are an infinite number of light sources that illuminate our observable universe, and the structure of this light is determined by the physical arrangement of the materials that occupy its space. As first defined in [5], the *plenoptic function* specifies the structure of light incident on an observer. The plenoptic function is fully specified by simultaneously resolving its 7 dimensions: the Cartesian coordinates of an image plane (2D), the light intensity variation with respect to wavelength λ (1D), the sampling of light over time (1D), and finally the observation of light at displaced viewpoints in the horizontal, vertical, and forward/backward direction (3D). Translating this introductory definition of the plenoptic function and applying it to the definition of snapshot hyperspectral imaging, a "snapshot" imaging spectrometer samples the light in a scene spatially in the image plane (2D) and spectrally (1D) at a single exposure, creating what is referred to as the 3D datacube. Other types of spectrometers (e.g., wiskbroom and pushbroom), perform scanning operations and sample a scene with multiple exposure times, which often yield motion artifacts. A comprehensive overview of the different architectures associated with imaging spectrometers is explained in [6].

Portability, as it pertains to our assessment of state-of-the-art, concerns not only the size of the devices under question but also their platform configuration as either being bench-top systems for use in a laboratory environment or deployable instruments for in-field analysis. As will be shown in the following sections, in-field analysis platforms have taken on new modalities to include not only hand-held devices, but also modules that can be integrated as payloads for unmanned autonomous vehicles (UAVs). This trend towards portability has driven device manufacturers over the past decade to encapsulate the enormous engineering and design efforts that would be required of building traditional large and expensive spectrometers used in typical scientific applications into marketable products with smaller form factors making spectroscopy more accessible to those of which who do not possess this domain specific expertise. There is, however, some expectation of the end user to have knowledge about their intended application as not all devices are "plug-and-play" and require some understanding of their mission requirements. In fact, there should also be a clear distinction between a fully stand-alone product as opposed to a secondary product that was meant to be integrated with other devices. These secondary products may or may not be out of reach of most end users, but there are third party firms that offer design and engineering related services that can be utilized for developing custom devices.

4.1 Spectral Filters

A large contributor to not only the reduction of the size, weight and power (SWaP) of hyperspectral imagers, but also to their optical system complexity, is by the integration of spectral filters. Traditionally, capturing multi-band images during a single exposure has been made possible by the so-called color filter array (CFA) for digital cameras. The most notable of these CFAs is the Bayer pattern [7] used to arrange RGB color filters on a grid of photodetectors. The spatial resolution is traded with spectral resolution while still allowing for the sensor to passively collect spectral information respective of the acuity of the human visual system. However, the limited spectral bands in the Bayer pattern severely restrict its use in a spectrometer due to its broad transmission bands and poor out-of-band blocking.

Fortunately, much progress has been made by various manufacturers in developing standardized processes for designing pixel-scale (μm) color and interference filters using common lithographic techniques. These spectral filters can be applied to either wafer-level glass and then bonded to the sensor or deposited directly onto the semiconductor substrate of the sensor [8]. The filter patterns available as of today range from: Bayer-like (area), stripe (row), mosaic [5] (per-pixel), line scan (wedge), or any other custom design needed. They may also have wide or narrow band passes or multivariate optical elements (MOEs) with varying spectral channels (e.g., UV, VIS, NIR, and SWIR). Table 1 shows a tradeoff between spatial versus spectral resolution. As the number of desired spectral bands increases, the spatial resolution, due to more pixels being used to spectrally sample the scene, decreases.

Table 1: The data in this table was taken from published information located in [9].

Pattern	Type	# Bands	Spectral Range [nm]	Spatial Resolution [px]
2x2	Mosaic	4	RGB+NIR	1024 x 544
4x4	Mosaic	16	460-630	512 x 272
5x5	Mosaic	25	600-1000	409 x 218
-	Bayer-like	32	600-1000	256 x 256
-	Stripe/Line Scan	100+	600-1000	2048 x length of scan
-	Stripe/Line Scan	150+	470-900	4096 x length of scan

The proper spectral bands must be identified for any application as it may be that only a few wavelengths or narrow spectral bands are relevant. Dielectric filter properties can be customized as edge filters (e.g., SWIR and LWIR) or single/multiple bandpass filters [10]. The study described in [10] shows the operation of a bandpass dichroic filter passing light emitted from a subject by means of fluorescence at a peak of 530nm, but blocking the excitation laser source at 470nm, while also rejecting out-of-band light. Further, the same study illustrates the improvement in sensor responsivity when the filter is constructed right on top of the sensor, including in the design the absorbing material and surface passivation layers, minimizing loses from filter/sensor interface. This process allows for compatibility of a wide range of materials including silicon (Si), silicon carbide (SiC), and indium gallium arsenide (InGaAs).

[5] In a mosaic filter, the cavity heights of each square grid are varied. Therefore, the wavelengths that are transmitted through the cavity are those that correspond to the resonant frequency of the etalon.

Several different hybrid pixelated filters (15μm feature size) were fabricated onto an optical substrate (e.g., glass) and then bonded to the focal plane array (FPA) of a SWIR detector showing an average alignment glass-to-FPA offset of 7.5μm (roughly half a pixel) to avoid crosstalk and other artifacts [11]. Further, two SWIR "scan" type implementations were developed, one with a standard line scan filter using a translation stage and the other a "snapscan" concept, where the FPA is translated through the projected image circle of the aperture with a piezoelectric translator [12]. Stripe pattern filters require either the object to move (e.g., conveyor or UAV) or the camera to move (e.g., on translation stage) and are not true snapshot systems. They also require that the framerate be adjusted for syncing purposes as the object-to-lens distance varies; and there could also be perspective deformations that occur from looking at the object from two different viewpoints that need to be corrected for [13]. Time constraints apply if a scene is expected to contain moving objects/platforms or high-speed events.

The takeaways from this section are as follows: first, selection of arbitrary wavebands is possible, limited only by the constraints of dielectric filtering (i.e., required feature sizes down to 2μm); second, filter patterns can be customized to produce any repeating pattern across the focal plane; third, patterns can be used for different sensor material types to accommodate varying spectral ranges; fourth, sensitivity to stray light, and optical complexity are reduced while maintaining passivity of light collection [8]. Finally, since the filters are applied to a glass substrate, one could use a filter with a line scan pattern to do a feasibility study and discover which bands are of actual interest to their application, and then work with a filter manufacturer to create a custom mosaic (i.e. snapshot) pattern that gives them the spectral information in the region most important to them.

4.2 Commercial Snapshot Hyperspectral Imagers

Since 2012, portable snapshot hyperspectral imagers began to be commercially available with their reduced size, weight, and power (SWaP) on the order of a typical digital single lens reflex (DSLR) camera, allowed for more compact designs at cost effective prices. The purported first known commercially available handheld snapshot hyperspectral imaging system was the Hyperspec RECON manufactured by Headwall in 2012. It operated in the VNIR (400 - 1000 nm) region and won an R&D 100 that year for its innovative design as did another snapshot hyperspectral imager, except the latter was not a portable device [14]. However, one group[15] claims RECON was not a true snapshot sensor because it had to perform an internal scan to acquire spectral information. What follows are descriptions of representative examples of snapshot spectral imagers and brief discussions those imagers applied to real problems.

4.2.1 XIMEA

The xiSpec line of cameras offered by XIMEA combine the semiconductor thin film processing expertise developed by imec with the compact package (just over an inch in LxWxH), lightweight (31g), and USB 3.0 interface of the xiQ cameras. The xiSpec cameras also draw their power (1.4W) from the USB 3.0 bus, ideal for integration as a payload on other platforms (e.g., UAV). This hyperspectral imager resembles a machine vision camera package unlike typical handheld DSLR cameras. Their image sensors are made by imec and contain all of the options listed in Table 1, to include spectral bands of NIR (600-900nm), VNIR (470-900nm), and VIS (470-630nm).

A study was conducted using a xiSpec camera with a 5x5 mosaic filter (VNIR w/ 25 bands) and a RGB camera analyzing the precision of deep neural networks (DNNs) for labeling scene components in an urban environment to resemble a typical surveillance application [16]. The field-of-views (FOVs) of the two cameras were aligned using bicubic interpolation and cropped giving a total of 28 spectral bands (+3 channels from RGB). They collected 40 images from a fixed perspective, and labeled the RGB images with one of 8 classes: car/truck, sky, building, road/gravel, tree/shrubbery, tram, water, and distant background. Several neural nets were analyzed with the highest error rate being 9.4% down to 0.9% using RGB and HSI data. Analysis of using the same network that gave 0.9% for RGB data alone, suffered from a 0.4% increase in error rate. They prove that RGB and HSI data together improves accuracy and that training on a relatively small dataset still yield high accuracy.

xiSpec cameras have also been applied to the biomedical field. Oxygenation monitoring of the hand was carried out using a xiSpec (5x5 VNIR filter w/ 25 bands) camera with a halogen light source where measurements were compared to a clinical system, an INVOS oximeter, as a reference [17]. Dynamic oxygenation changes were determined with the HSI camera and INVOS system at different regional locations on the patients hand and showed to be in good agreement. Passively sampling oxygenation transport is critical as blood profusion and oxygen distribution is a dynamic process where information is lost if done over time. A second study done by a different group, used xiSpec (4x4 VIS filter w/ 16 bands) camera for skin oxygen saturation monitoring [18]. The measurements from the HSI camera were validated using reference color samples and *in vivo* during finger arterial occlusion tests, which were in good agreement within the 500-630 nm range. Another group using the same xiSpec camera as the previous, evaluated the use of the camera, paired with an inverse Monte Carlo algorithm, to take spatial and temporal measurements during arterial and venous occlusion protocols applied to the forearm. The conclusion was that the device could be used in carrying out skin tissue blood volume and oxygenation measurements [19]. Finally, two similar studies were carried out with both using the same xiSpec (4x4 VIS filter w/ 16 bands) camera. One developed a method to emulate the spectral range and resolution of any HSI camera based on in-vivo data from spatial frequency domain spectroscopy (SFDS) spectra and validated their results against measurements from the HSI camera [20]. The other evaluated the use of different illumination patterns of red, green, and blue using a digital light processing (DLP) projector of an arterial occlusion and release protocol on the forearm [21].

4.2.2 Specim

The SpecimIQ is a portable handheld device in a package very similar to a typical DSLR camera but larger in size, and was designed to enable in-field hyperspectral analysis. It has an embedded processor and integrated software with a user interface that allows for data processing to be done directly on the camera. It is battery powered, operates in the VNIR range (400-1000 nm), has a spatial resolution of 512x512, and a total of 204 spectral bands at 7nm resolution. Its operational range is from 10cm to tens of meters and has a FOV of 40° at 1m. It has a recording time of 0.6s-300s depending on illumination level. A feasibility study was carried out on the SpecimIQ, where it underwent different testing conditions on laboratory targets and artworks in hopes of pointing

out its strengths and weaknesses for use in the cultural heritage field [22]. [6]

Laboratory measurements included: imaging a colorimetric reference standard simultaneously with a white target, then comparing the reflectance spectral data from the 3D datacube to the reference reflectance data; carrying out a wavelength calibration check against a Holmium Oxide reference target and comparing results with another hyperspectral scanner used for high-precision hyperspectral measurements on paintings; testing its spatial resolution against a USAF reference target; and measurements on a replica painting for pigment classification. Colorimetric results were in good agreement with reference data with the largest deviations coming from the yellow line, proving acceptable for its use in non-precision colorimetric reconstruction. Wavelength calibration results were in very good agreement between the two devices. The spatial resolution of the device is approximately 0.25 line pairs per millimeter at a distance of 60 cm. The pigments were correctly classified except for areas were illumination wasn't present. [7]

Field measurements were taken on the lunette in the San Marco museum cloister. The instrument proved successful as most pigments were identified including smalt used in blue pigments. The reflectance data of green pigments increased for wavelengths longer than 650 nm indicating a mixture of pigments between yellow and blue. The authors of the study used principle component analysis (PCA) on spectral data from 410-900nm and demonstrated through their findings: highlighting different spectral responses, revealing cracks and dark areas unseen from the naked eye, and inhomogeneous patches of color.

4.2.3 Pixelteq

Pixelteq possess semiconductor thin film processing expertise and uses the technology they have developed in-house [23] on their own devices. The PixelSensor contains micro-patterned dichroic pixel-wise filters that are deposited directly at the wafer level and has 8 spectral channels in a 3x3 array. The sensor is approximately 9x9mm and can be surface or socket-mounted, or comes with an evaluation kit which includes the electronic readout circuits, software, and optics for rapid prototyping [24]. The PixelCam camera is like the xiSpec cameras in that it is packaged as a machine vision camera. It is portable, but not handheld like the SpecimIQ. The PixelCam is classified as a multispectral imager containing 3-9 spectral bands in VNIR (2MP or 4MP options) or NIR+SWIR (640x512 resolution) regions. Depending upon the spectral bands chosen, the image sensor packaged with the PixelCam is either a Si CCD with a 7.4μm pixel pitch or a InGaAs sensor with a 25μm pixel pitch. The device is approximately twice as large as the xiSpec cameras, and weights 377g. The VNIR version provides a GigE interface and the NIR+SWIR device provides a Camera Link 14-bit interface.

Two studies were carried out one where a pixel-sized 3x3 repeating pattern SWIR filter made by Pixelteq was mounted onto a COTS FPA for spectral response characterization [25] and the other demonstrating an image processing task of demosaicking the aforementioned Pixelteq filter to reconstruct the spectral images recorded by the FPA, keeping intact its resolution from spatially

[6] It should be noted that the measurements were made in a line scan fashion as this device is not a true snapshot imager, but was included in this section due to its innovative design.

[7] Interestingly, the authors analyzed the presence of underwritings by extracting an image at 900 nm, clearly showing writing structure under the more transparent pigments and paint layers.

subsampled and incomplete spectral data [26]. In order to reduce crosstalk between adjacent pixels, an absorbing material was placed in the space between the filters (exactly the same technique employed by [11] above).

4.2.4 AlphaNOV

The GoSpectro device developed by AlphaNOV was a SPIE PRISM awards finalist in 2015 for their innovative design of a secondary product that can be attached to smartphones or tables enabling in-field spectroscopic analysis. Depending upon the imaging sensor of the handheld device, the spectral range is 400-750 nm (VIS), with 10 nm resolution, and acquires spectral images at 10 frames per second [27].

4.2.5 LinkSquare

Linksquare [28] developed by Stratio Inc. is a pencil-like imaging spectrometer operating at 400-675 nm, WIFI enabled, weights 140 g, and costs approximately $300. The device transmits its measurements to either a smartphone or computer wirelessly for analysis. It has proven to accurately detect bio-samples of bananas, meat, and human hands. Startio provides the users of their product access to their optimized machine learning algorithms for material identification. A unique aspect of this manufacturer-to-customer connection is that it allows for all the data acquired with customer LinkSquare devices to be used in training deep learning algorithms for further improvement of material identification.

4.3 TRI Analyzer

The Transmission, Reflection, and Intensity (TRI)-Analyzer is a smartphone-based imaging spectrometer comprising of three spectral sensing modalities with two independent fiber-delivered light paths and the imaging sensor. Its optical design is unlike any other device mentioned thus far. Most of the housing and optical holders are 3D printed where a friction fit between two halves of the housing is enough to hold the analyzer together while also maintaining a proper optical alignment. The two sources of illumination are fiber delivered to the sample chamber utilizing a 532nm laser diode and the smartphones flash element. In the laser path, optics are put in place to collect light from fluorescence, transmission, and reflections from the subject and coupled into a fiber. In the smartphone flash optical path, the collection fiber is terminated wtih a glass capillary tube to increase its light collection from the broad spectrum of the flash source. The collected light from the two optical paths are then passed through a transmission grating and finally through the aperture of the smartphone camera for imaging.

4.4 Scientific Snapshot Hyperspectral Imagers

The systems described in this section represent the field of active research and are still considered relevant to establishing the leading edge in snapshot hyperspectral imaging. Some of the systems listed in this section may become a commercial products in the next 5 years.

4.4.1 VTT Technical Research Center of Finland

VTT research group has been actively researching cost-effective hyperspectral imaging technology since 2006. In 2011 and 2013, they developed a miniature tunable spectral imager utilizing a Fabry-Perot interferometer (FPI) with a spectral range from 400-1000nm accompanied by an RGB CMOS image sensor for deployment as a payload to the Aalto-1 3U-cubesat [29, 30].

Two years later they utilized the technical expertise they developed for the CubeSat application and integrated the tunable FPI device as a payload in a UAV [31]. It had on-board calibration, operated in the 400-900 nm range, and consisted of 10-40 nm spectral resolution. The goal was to study forest inventory, crop biomass and nitrogen distributions, and environmental status of natural water applications.

A year later, the same group presented a micro-opto-electro-mechanical (MOEMS) FPI for NIR (800 nm-1050 nm) sensing to enable low-cost silicon-based spectroscopy [32]. The unique monolithic surface-micromachined MOEMS construction expertise they developed gives the device robustness to mechanical shock of up to 18,000 g's while also being insensitive to vibrational effects that may distort optical measurements. The optical aperture size was 1.5 mm enabling single-point VNIR microspectrometers or miniature hyperspectral imagers. A year after this study, they presented a MOEMS FPI with an increased aperture diameter of 4 mm, central wavelengths of 500 nm and 650 nm, and spectral resolution of 10 nm and 12 nm respectively [33].

The technology and expertise the VTT researchers attained from the CubeSat and UAV projects allowed for them to develop a miniaturized microelectromechanical (MEMS) FPI for CO_2 gas detection using a cell phone [34]. The sensor connected to the smartphone via Bluetooth and drew its power from 2 coin cell batteries. The optical components were an infrared emitter, sapphire lens, long pass filter, MEMS FPI, and lead selenide (PbSe) detector. The device operated from 4000 nm to 4200 nm due to carbon dioxide having strong absorptions in the wavelength range of 4200-4400 nm. In a collaborative effort by VTT and others [35], VTT researchers delivered a piezo-actuated tunable FPI operating in the 430-800 nm range with a 10 nm resolution for deployment as a payload on the PICo-satellite for atmospheric and space observations.

At the time of this writing, VTT researchers have developed tunable FPI optical filters covering wavelengths from UV-VIS, SWIR, and LWIR with continuous efforts to commercialize the technology and expertise previously developed in other projects. In an overview article of VTT's work on FPI technologies for hyperspectral imaging and mobile sensing platforms [36], they give an account of their R&D efforts aimed at increasing the performance of silicon-air MEMS FPI processes; including layer depositions, and stress control and release methods that have allowed for NIR and MWIR range devices to be fabricated. Their efforts have ultimately led to the development of a MEMS tunable FPI hyperspectral imaging sensor operating from 450-550nm with a spectral resolution of 8-15nm that can be coupled to a smartphone for in-field spectroscopic measurements.

4.4.2 Active Research

Computational Imaging (CI) techniques and their application to spectroscopy are now common. Computational techniques use optical coding followed by computational decoding [37]. The coded aperture snapshot spectral imager (CASSI) developed on behalf of a DARPA funded research

project, provided experimental verification of the use of compressive sensing for capturing the 3D datacube [38]. As a continuation of that work, the same group expanded upon the original system and demonstrated that they could image a dynamic scene at videos rates [39].

In recent years, there has been tremendous growth of the use of snapshot spectral imaging being applied to the biomedical industry to include: retinal imaging [40–42], *in-vivo* identification of drusen to understanding macular degeneration [43], and in-vivo detection of oxy-hemoglobin with a snapshot hyperspectral endoscope [44]. Medical imaging has also seen a boost of the use of image mapping spectrometers developed for hyperspectral microscopy [45, 46] and even for visualizing the blood transport in the brain to better understand neurovascular coupling to cerebral metabolism [47]. For a more comprehensive overview of medical hyperspectral imaging technology and its applications, please refer to the following articles [48, 49].

5 Potential Applications

The applications presented in the following sections are not unique in the sense that researchers and equipment manufacturers are already addressing these issues with laboratory and scientific-grade instruments. Rather, these are applications where we see immediate benefit given the *portability* of handheld, snapshot implementation of VNIR imaging technology. We expect other applications will come to fruition when the technology becomes more widely available to the general consumer market[8] VNIR systems are becoming cheaper and more available and come packaged with processing software to automate the detection and analysis of materials. In addition, the sensors are becoming smaller and lighter with Size, Weight, and Power (SWaP) specifications making them able to fly on Unmanned Airborne Vehicles (UAVs.) In some applications, such as forensics and art analysis, it is the pigments of fabric dyes or paints[52] that are of interest.

5.1 Crime-scene forensics

An important aspect of gathering evidence during a criminal investigation is forensic analysis. Forensic scientists use photographic evidence to record such things as the location of potentially important objects (e.g., victims clothing, murder weapons, etc.) and patterns (e.g., blood splatter, fingerprints, etc.) at a crime scene. Physical evidence that require chemical or colorometric analysis have to be removed from the scene and brought back to a laboratory, which increases the amount of time needed to link a potential suspect to a crime. Further, removal of evidence from a crime scene may alter the physical state of that evidence and, thus, either render it useless or otherwise lead to errors in the analysis. A portable HSI device provides to a crime scene investigator the unique ability to make *non-contact*[53, 54] chemical analysis at the scene while at the same time imaging its location within a crime scene.

5.2 Counter Denial and Deception

The detection of camouflage and plastics can help warfighters detect the presence of camps associated with an enemy, insurgents, or drug traffickers, as well as ordinance and dismounts. The detection of plastics, camouflage, synthetic fabrics and other man-made materials has traditionally been performed by SWIR sensors because many of those materials are hydrocarbon-based and tend to exhibit distinguishing features (relatively sharp dips in spectral response) at 1.2 um and 1.7 um. However, it is possible to distinguish certain man-made materials from natural materials based on their spectral signatures in the VNIR. (A demonstration of using VNIR HSI to detect camouflage is shown in the Appendix.) Our preliminary examination of this capability indicates that detection in the VNIR is possible, but not as robust as in the SWIR. In the absence of characteristic hydrocarbon features in the SWIR, the detection of plastics in the VNIR-only appears to be more sensitive to variation in illumination. A detection system designed to detect such materials using only the VNIR would need to include techniques to compensate for illumination variations or to include a large variety of illumination conditions in the spectral library.

[8] Two classic examples of this are the use of webcams by amateur astronomers[50] or smartphone apps that use the build-in sensors (e.g., accelerometers)[51] for purposes not originally intended by the manufacturer.

5.3 Search and Rescue

This application is related to the detection of plastics and hydrocarbon-based materials. A downed aircraft, flame-retardant material (e.g., Nomex) worn by aircraft crew, life-vests, debris etc., have in common, that they are made or painted with hydrocarbon-based materials. As with the detection of plastics, the detection of these materials is possible in the VNIR, though likely not as robust as detection in the SWIR. An advantage to having a compact, self-contained snapshot spectral imager is the ability to mount the camera on small UASs that can be carried by ground teams into the vicinity of where the downed aircraft, lost hikers, etc., were last scene and sent aloft to aid in the search. Such a system would be of particular help in rugged terrain where it may be too time consuming to conduct the search solely on foot. Furthermore, a snapshot system also has a distinct advantage over existing UAS-mounted line-scanning systems in that it can loiter over an area of interest without needing motion to form an image.

5.4 Medicine

Hyperspectral imaging has been used to identify anomalous or diseased tissue and early disease detection. VNIR imaging could be used to detect early forms of cancer or retinal disease either in vitro or via tissue samples. Uses[55–60] have been reported or been suggested in brain tissue metabolic and hemodynamic monitoring, red blood cell counting, histopathology and cytology, dermatology, pressure ulcers, colorectal and gastric cancer, residual tumor identification during surgery, cervical cancer, burn wounds, diabetic foot, tumor hypoxia, skin cancer, hemorrhagic shock, skin bruises, ophthalmology, laparoscopic surgery, intestinal ischemia, endoscopy, atherosclerosis, prostate cancer, laryngeal disorders, cholecystectomy, ovarian cancer, leucocyte pathology, and nerve fiber identification.

5.5 Security & Law Enforcement

Cameras used for security (e.g., shopping malls, banks, perimeters of military bases and government facilities) and law enforcement (e.g., police cruiser cameras and bodycams) are either 3-color RGB video and monochromatic near-infrared[61, 62], which are limited to literal analysis, such as to identify criminal perpertrators, read license plates, or the make, model, and color of a vehicle. Adding 10's, if not 100's of spectral bands would enable the ability to uniquely identify clothing, car paints, and possibly chemical substances such as narcotics, explosives, and hazardous materials. Spectral imaging could also be used to identify spectral "tags" attached to suspect vehicles or items that are designed to be invisible to the unaided eye. One could imagine a police officer using a hyperspectral cell phone camera to image the paint on a vehicle suspected of being involved in a hit-and-run to see if the paint matches samples found on the struck vehicle.

5.6 First responders

First responsers, such as police officers, emergency medical technicians (EMTs), and firefighters, can find themselves in situations where hand-portable spectral imaging could have a huge impact

on how quickly to move into a disaster area or help assess physical injuries to vicitms. An accident at an industrial facility could result in the dispersal of hazardous chemicals that a spectral imager could detect and possibly identify, thus informing the rescuers as to the necessary safety protocols to follow. As mentioned above in Section 5.4, spectral technology has many applications in clinical medicine; imagine being able to quickly assess chemical burns and/or contamination on a victims body by an EMT assessing the condition of an accident victim at the scene.

6 Technical Challenges

The technical characteristics of smaller, cheaper hyperspectral instruments determines their viability for specific task. Of importance are the instrument's signal-to-noise ratio (SNR), spatial, spectral resolution and processing steps required to detect materials. Instruments and the algorithms used to process the data need to be robust and automatically adapt to varying illumination and environmental conditions.

Data processing and material detection could be designed to work in a variety of background environments. For example, if foliage is a likely scene background and camouflage is the target material, algorithms such as VANTAGE[63] could be used to correct for changing illumination levels and correct the data to reflectance. VANTAGE detects the presence of foliage in the imagery using normalized difference vegetation indices (NDVI)[64]. It then finds the mean of the foliage-like pixels and compares to a reference reflectance spectrum of mean foliage to determine the correction factors needed to convert the sensor data (in radiance) to reflectance. This methodology could be adapted to non-foliage environments as long as the dominant background has a predictable spectral signature. In cases where there are man-made objects in the scene, the atmospheric compensation code, QUAC (QUick Atmospheric Compensation)[65] may be appropriate. QUAC first uses the band-by-band minimum to compute an offset term. It then finds the mean of representative spectra of non-foliage materials in the scene and compares to the mean of a reference reflectance library of materials. Like in the case of VANTAGE, this comparison produces a multiplicative correction term to convert the sensor data from radiance to reflectance.

In some cases, a more direct approach of using raw, dark-subtracted sensor data to collect signatures could work rather than converting the data to reflectance. In that case, the spectrum of a material of interest is collected directly from the dark-subtracted raw sensor data and used as the reference signature to detect other similar materials in the same scene or subsequent scenes. This technique is the simplest and easiest to implement and can work if the illumination does not change significantly, and/or the target material is spectrally distinct from clutter and background materials.

There is also the computational cost of performing more advanced functions with the acquired data, such as material characterization and identification. The ability to perform on-board calculuations will largely be a function of microprocessing power and the data volume. It is expected that the first generation of portable spectral imagers will have limited spatial dimensions to accomodate 10's to 100's of bands for greater spectral fidelity. It should be noted as well that increasing the number of spectral bands will result in lower SNR per band, which could require additional image processing to mitigate noise and other artifacts.

7 Summary and Conclusions

The technology to create portable, snapshot hyperspectral cameras is already here. It will only be a few years before the technology will appear in commercial devices, such as cell phone and palm-sized cameras. We have presented in this report an overview of the current state-of-the-art in VNIR spectral imaging technology with an eye towards smaller, portable devices and the potential applications of the technology provided certain technical challenges are overcome. We expect that first-adopters and the Do-it-Yourself (DIY) community will come up with applications that neither we nor the vendors have thought of, much like what happened with smart phones. There is a need to continue to monitor the technology and develop algorithms and prototype hardware to avoid technical surprise, such as foreign adversaries using the technology for clandestine collection or criminals intent on defeating security measures.

References

[1] "Nano-hypspec product data sheet." https://cdn2.hubspot.net/hubfs/145999/June%202018%20CollateralNanoHyperspec0118.pdf?t=1535573251139, June 2018.

[2] "VNIR HSI technology can be integrated with consumer devices." https://www.photonics.com/Article.aspx?AID=63081.

[3] M. T. Eismann, *Hyperspectral Remote Sensing*. SPIE, 2012.

[4] P. Hauff, "An overview of vis-nir-swir field spectroscopy as applied to precious metals exploration," vol. 80001, 01 2008.

[5] E. H. Adelson and J. R. Bergen, "The plenoptic function and the elements of early vision," in *Computational Models of Visual Processing*, pp. 3–20, MIT Press, 1991.

[6] N. A. Hagen, L. S. Gao, T. S. Tkaczyk, and R. T. Kester, "Snapshot advantage: a review of the light collection improvement for parallel high-dimensional measurement systems," *Optical Engineering*, vol. 51, pp. 51 – 51 – 8, 2012.

[7] B. E. Bayer, "Color Imaging Array," 1975. US3971065A.

[8] E. V. Chandler, D. E. Fish, and K. J. Evanson, "Real-time compact multispectral imaging solutions using dichroic filter arrays," vol. 9022, pp. 9022 – 9022 – 6, 2014.

[9] IMEC, "Hyperspectral Imaging Sensor Data." https://www.imec-int.com/en/hyperspectral-imaging.

[10] E. V. Chandler and D. E. Fish, "Compact multispectral photodiode arrays using micropatterned dichroic filters," vol. 9101, pp. 9101 – 9101 – 9, 2014.

[11] Y. Karni, M. Nitzani, E. Jacobsohn, I. Grimberg, S. Gliksman, A. Giladi, L. Krasovitski, E. Avnon, L. B. I. Hirsh, I. Lukomsky, L. Shkedy, R. Fraenkel, I. Shtrichman, P. Gonzalez, and A. Lambrechts, "Spatial and spectral filtering on focal plane arrays," vol. 10624, pp. 10624 – 10624 – 10, 2018.

[12] P. Gonzalez, J. Pichette, B. Vereecke, B. Masschelein, L. Krasovitski, L. Bikov, and A. Lambrechts, "An extremely compact and high-speed line-scan hyperspectral imager covering the swir range," vol. 10656, pp. 10656 – 10656 – 9, 2018.

[13] A. L. Julien Pichette, Wouter Charle, "Fast and compact internal scanning cmos-based hyperspectral camera: the snapscan," vol. 10110, pp. 10110 – 10110 – 10, 2017.

[14] "First instant hyperspectral camera for live samples," 2012.

[15] B. Geelen, N. Tack, and A. Lambrechts, "A snapshot multispectral imager with integrated tiled filters and optical duplication," vol. 8613, pp. 8613 – 8613 – 13, 2013.

[16] L. Cavigelli, D. Bernath, M. Magno, and L. Benini, "Computationally efficient target classification in multispectral image data with deep neural networks," vol. 9997, pp. 9997 – 9997 – 12, 2016.

[17] J. R. Bauer, K. van Beekum, J. Klaessens, H. J. Noordmans, C. Boer, J. Y. Hardeberg, and R. M. Verdaasdonk, "Towards real-time non contact spatial resolved oxygenation monitoring using a multi spectral filter array camera in various light conditions," vol. 10489, pp. 10489 – 10489 – 9, 2018.

[18] U. Rubins, Z. Marcinkevics, J. Cimurs, A. Grabovskis, and E. Kviesis-Kipge, "Snapshot hyperspectral system for noninvasive skin blood oxygen saturation monitoring," vol. 10685, pp. 10685 – 10685 – 8, 2018.

[19] M. Ewerlöf, M. Larsson, and E. G. Salerud, "Spatial and temporal skin blood volume and saturation estimation using a multispectral snapshot imaging camera," vol. 10068, pp. 10068 – 10068 – 12, 2017.

[20] R. B. Saager, M. L. Baldado, R. A. Rowland, K. M. Kelly, and A. J. Durkin, "Method using *in vivo* quantitative spectroscopy to guide design and optimization of low-cost, compact clinical imaging devices: emulation and evaluation of multispectral imaging systems," *Journal of Biomedical Optics*, vol. 23, pp. 23 – 23 – 12, 2018.

[21] T. Strömberg, R. B. Saager, G. T. Kennedy, I. Fredriksson, G. Salerud, A. J. Durkin, and M. Larsson, "Spatial frequency domain imaging using a snap-shot filter mosaic camera with multi-wavelength sensitive pixels," vol. 10467, pp. 10467 – 10467 – 11, 2018.

[22] C. Cucci, A. Casini, L. Stefani, M. Picollo, and J. Jussila, "Bridging research with innovative products: a compact hyperspectral camera for investigating artworks: a feasibility study," vol. 10331, pp. 10331 – 10331 – 13, 2017.

[23] P. E. Buchsbaum and M. J. Morris, "Method for making monolithic patterned dichroic filter arrays for spectroscopic imaging," 2000. US6638668B2.

[24] PIXELTEQ, "PixelSensor Datasheet," 2018. https://pixelteq.com/pixel-sensor/.

[25] M. R. Kutteruf, M. K. Yetzbacher, M. J. Deprenger, K. M. Novak, C. A. Miller, and A. Kanaev, "9-band swir multispectral sensor providing full-motion video," vol. 9076, pp. 9076 – 9076 – 12, 2014.

[26] A. V. Kanaev, M. Rawhouser, M. R. Kutteruf, M. K. Yetzbacher, M. J. DePrenger, K. M. Novak, C. A. Miller, and C. W. Miller, "Demosaicking for full motion video 9-band swir sensor," vol. 9104, pp. 9104 – 9104 – 8, 2014.

[27] Alphanov, "Gospectro datasheet," 2015. http://www.alphanov.com/56-spectroscopy-gospectro—spectrometer-for-smartphone.html.

[28] F. Cai, D. Wang, M. Zhu, and S. He, "Pencil-like imaging spectrometer for bio-samples sensing," *Biomed. Opt. Express*, vol. 8, pp. 5427–5436, Dec 2017.

[29] R. Mannil, A. Näsilä, J. Praks, H. Saari, and J. Antila, "Miniaturized spectral imager for aalto-1 nanosatellite," vol. 8176, pp. 8176 – 8176 – 8, 2011.

[30] R. Mannila, A. Näsilä, K. Viherkanto, C. Holmlund, I. Näkki, and H. Saari, "Spectral imager based on fabry-perot interferometer for aalto-1 nanosatellite," vol. 8870, pp. 8870 – 8870 – 9, 2013.

[31] H. Saari, I. Pölönen, H. Salo, E. Honkavaara, T. Hakala, C. Holmlund, J. Mäkynen, R. Mannila, T. Antila, and A. Akujärvi, "Miniaturized hyperspectral imager calibration and uav flight campaigns," vol. 8889, pp. 8889 – 8889 – 12, 2013.

[32] A. Rissanen, R. Mannila, M. Tuohiniemi, A. Akujärvi, and J. Antila, "Tunable moems fabry-perot interferometer for miniaturized spectral sensing in near-infrared," vol. 8977, pp. 8977 – 8977 – 8, 2014.

[33] A. Rissanen, A. Langner, K. H. Viherkanto, and R. Mannila, "Large-aperture moems fabry-perot interferometer for miniaturized spectral imagers," vol. 9375, pp. 9375 – 9375 – 8, 2015.

[34] R. Mannila, R. Hyypiö, M. Korkalainen, M. Blomberg, H. Kattelus, and A. Rissanen, "Gas detection with microelectromechanical fabry-perot interferometer technology in cell phone," vol. 9482, pp. 9482 – 9482 – 9, 2015.

[35] H. Saari, A. Näsilä, C. Holmlund, R. Mannila, I. Näkki, H. J. Ojanen, D. Fussen, D. P. P. Demoulin, E. Dekemper, and F. Vanhellemont, "Visible spectral imager for occultation and nightglow (vision) for the picasso mission," vol. 9639, pp. 9639 – 9639 – 11, 2015.

[36] A. Rissanen, B. Guo, H. Saari, A. Näsilä, R. Mannila, A. Akujärvi, and H. Ojanen, "Vtt's fabry-perot interferometer technologies for hyperspectral imaging and mobile sensing applications," vol. 10116, pp. 10116 – 10116 – 12, 2017.

[37] O. Cossairt, M. Gupta, and S. K. Nayar, "When does computational imaging improve performance?," *IEEE Transactions on Image Processing*, vol. 22, pp. 447–458, Feb 2013.

[38] A. Wagadarikar, R. John, R. Willett, and D. Brady, "Single disperser design for coded aperture snapshot spectral imaging," *Appl. Opt.*, vol. 47, pp. B44–B51, Apr 2008.

[39] A. A. Wagadarikar, N. P. Pitsianis, X. Sun, and D. J. Brady, "Video rate spectral imaging using a coded aperture snapshot spectral imager," *Opt. Express*, vol. 17, pp. 6368–6388, Apr 2009.

[40] W. R. Johnson, D. W. Wilson, W. Fink, M. S. Humayun, and G. H. Bearman, "Snapshot hyperspectral imaging in ophthalmology," *Journal of Biomedical Optics*, vol. 12, pp. 12 – 12 – 7, 2007.

[41] L. Gao, R. T. Smith, and T. S. Tkaczyk, "Snapshot hyperspectral retinal camera with the image mapping spectrometer (ims)," *Biomed. Opt. Express*, vol. 3, pp. 48–54, Jan 2012.

[42] H. Li, W. Liu, B. Dong, J. V. Kaluzny, A. A. Fawzi, and H. F. Zhang, "Snapshot hyperspectral retinal imaging using compact spectral resolving detector array," *Journal of Biophotonics*, vol. 10, no. 6-7, pp. 830–839.

[43] N. Lee, J. Wielaard, A. A. Fawzi, P. Sajda, A. F. Laine, G. Martin, M. S. Humayun, and R. T. Smith, "In vivo snapshot hyperspectral image analysis of age-related macular degeneration," in *2010 Annual International Conference of the IEEE Engineering in Medicine and Biology*, pp. 5363–5366, Aug 2010.

[44] R. T. Kester, N. Bedard, L. S. Gao, and T. S. Tkaczyk, "Real-time snapshot hyperspectral imaging endoscope," *Journal of Biomedical Optics*, vol. 16, pp. 16 – 16 – 13, 2011.

[45] L. Gao, R. T. Kester, N. Hagen, and T. S. Tkaczyk, "Snapshot image mapping spectrometer (ims) with high sampling density for hyperspectral microscopy," *Opt. Express*, vol. 18, pp. 14330–14344, Jul 2010.

[46] Z. Lavagnino, J. Dwight, A. Ustione, T.-U. Nguyen, T. S. Tkaczyk, and D. W. Piston, "Snapshot hyperspectral light-sheet imaging of signal transduction in live pancreatic islets," *Biophysical Journal*, vol. 111, 2016.

[47] J. Pichette, A. Laurence, L. Angulo, F. Lesage, A. Bouthillier, D. K. Nguyen, and F. Leblond, "Intraoperative video-rate hemodynamic response assessment in human cortex using snapshot hyperspectral optical imaging," *Neurophotonics*, vol. 3, pp. 3 – 3 – 9, 2016.

[48] G. Lu and B. Fei, "Medical hyperspectral imaging: a review," *Journal of Biomedical Optics*, vol. 19, pp. 19 – 19 – 24, 2014.

[49] Q. Li, X. He, Y. Wang, H. Liu, D. Xu, and F. Guo, "Review of spectral imaging technology in biomedical engineering: achievements and challenges," *Journal of Biomedical Optics*, vol. 18, pp. 18 – 18 – 29, 2013.

[50] D. Down, "Webcam imaging: Turn a simple camera on the solar system for stunning pictures of the planets and moon." `http://skyatnightmagazine.com/feature/astrophotography-guide/webcam-imaging`, December 2010.

[51] "All the sensors in your smartphone and how they work." `https://gizmodo.com/all-the-sensors-in-your-smartphone-and-how-they-work-1797121002`, July 2017.

[52] K. Ferreira, A. Oliveira, A. Goncalves, and J. Gomes, "Evaluation of hyperspectral imaging visible/near infrared spectroscopy as a forensic tool for automotive paint distinction," *Forensic Chemistry*, vol. 5, pp. 46 – 52, 2017.

[53] S. Cadd, B. Li, P. Beveridge, W. T. O'Hare, A. Campbell, and M. Islam, "A comparison of visible wavelength reflectance hyperspectral imaging and acid black for the detection and identification of blood stained fingerprints," *Science and Justice*, vol. 56, pp. 247–255, 2016.

[54] S. Cadd, B. Li, P. Beveridge, W. T. O'Hare, A. Campbell, and M. Islam, "The non-contact detection and identification of blood stained fingerprints using visible wavelength reflectance hyperspectral imaging: Part 1," *Science and Justice*, vol. 56, pp. 181–190, 2016.

[55] S. V. Panasyuk, S. Yang, D. V. Faller, D. Ngo, R. A. Lew, J. E. Freeman, and A. E. Rogers, "Medical hyperspectral imaging to facilitate residual tumor identification during surgery," *Cancer Biology & Therapy*, vol. 6, no. 3, pp. 439–446, 2017.

[56] M. A. Calin, S. V. Parasca, D. Savastru, and D. Manea, "Hyperspectral imaging in the medical field: Present and future," *Applied Spectroscopy Reviews*, vol. 49, no. 6, pp. 435–447, 2014.

[57] F. Vasefi, N. MacKinnon, and D. Farkas, "Chapter 16 - hyperspectral and multispectral imaging in dermatology," in *Imaging in Dermatology* (M. R. Hamblin, P. Avci, and G. K. Gupta, eds.), ch. 16, pp. 187–201, Boston: Academic Press, 2016.

[58] F. Fereidouni, C. Griffin, A. Todd, and R. Levenson, "Multispectral anlaysis tools can increase utility of rgb color images in histology," *Journal of Optics*, vol. 20, no. 4, p. 044007, 2018.

[59] X. Liu, M. Zhou, S. Qiu, L. Sun, H. Liu, Q. Li, and Y. Wang, "Adaptive and automatic red blood cell counting method based on microsopic hyperspectral imaging technology," *Journal of Optics*, vol. 19, no. 12, p. 124014, 2017.

[60] G. Lu and B. Fei, "Medical hyperspectral imaging: a review," *Journal of Biomedical Optics*, vol. 19, no. 1, 2015.

[61] `https://www.pcmag.com/reviews/home-security-cameras`. This link provides a representative sampling of the technology currently available to consumers.

[62] V. Hung, S. Babin, and J. Coberly, "A Market Survey on Body Worn Camera Technologies," Tech. Rep. 250381, The Johns Hopkins University Applied Physics Laboratory, November 2013.

[63] E. Crist, J. Cederquist, and J. Nunez, "VANTAGE-automatic atmospheric compensation for hyperspectral target detection," in *Proceedings of the IRIS CC&D Conference*, March 2000.

[64] "Measuring vegetation (NDVI & EVI) normalized difference vegetation index (NDVI)." `https://earthobservatory.nasa.gov/Features/MeasuringVegetation/measuring_vegetation_2.php`, August 2000.

[65] L. S. Bernstein, S. M. Adler-Golden, R. L. Sundberg, R. Y. Levine, T. C. Perkins, A. Berk, A. J. Ratkowski, G. Felde, and M. L. Hoke, "Validation of the QUick Atmospheric correction (QUAC) algorithm for VNIR-SWIR multi- and hyperspectral imagery," in *Proceedings of SPIE*, vol. 5806, pp. 5806 – 5806 – 1, 2005.

[66] D. Manolakis, M. Pieper, E. Truslow, T. Cooley, and M. B. et al, "The remarkable success of adaptive cosine estimator in hyperspectral target detection," in *Algorithms and Technologies for Multispectral, Hyperspectral, and Ultraspectral Imagery XIX*, vol. 8743, SPIE, SPIE, May 2013.

[67] Ximea, "Mq022hg-im-sm4x4-vis,"

[68] Ximea, "Mq022hg-im-sm5x5-nir,"

[69] Ximea, "Mq022hg-im-ls150-visnir,"

[70] Ximea, "Mq022hg-im-ls100-nir,"

[71] Specim, "Specim iq,"

[72] "Pixelcam™ oem multispectral cameras." `https//www.pixelteq.com/pixelcam`.

[73] Alphanov, "Gospectro: Smartphone spectrometer,"

[74] Stratio, “Linksquare,”

[75] PhotonFocus, “Mv0-d2048x1088-c01-hs03-160-g2,”

[76] PhotonFocus, “Mv0-d2048x1088-c01-hs02-160-g2,”

[77] PhotonFocus, “Mv1-d2048x1088-hs05-96-g2,”

[78] PhotonFocus, “Mv1-d2048x1088-hs01-96-g2,”

[79] H. Wu, F. G. Haibach, E. Bergles, J. Qian, C. Zhang, and W. Yang, “Miniaturized handheld hyperspectral imager,” vol. 9101, pp. 9101 – 9101 – 6, 2014.

[80] S. T. Huawen (Owen) Wu, Hui Li, “New generation handheld hyperspectral imager,” vol. 10156, pp. 10156 – 10156 – 6, 2016.

[81] BaySpec, “Oci-2000 snapshot handheld hyperspectral imager,”

[82] 3DOne, “Hyperview,”

[83] “Trutag technologies teams up with the state of hawaii at the bio international convention.” https://www.hinaleaimaging.com/trutag-technologies-teams-up-with- the-state-of-hawaii-at-the-bio-international-convention/, May 2018.

[84] E. Herrala, J. T. Okkonen, T. S. Hyvarinen, M. Aikio, and J. Lammasniemi, “Imaging spectrometer for process industry applications,” vol. 2248, pp. 2248 – 2248 – 8, 1994.

[85] J. Chen, F. Cai, R. He, and S. He, “Experimental demonstration of remote and compact imaging spectrometer based on mobile devices,” vol. 18, p. PMC6068658, 2018.

[86] Hamamatsu, “C12666ma,”

[87] Tittle, “S200 hyp,”

[88] Cubert, “S185 - hyperspectral se,”

[89] Cubert, “S 496 - hyperspectral,”

[90] Cubert, “Q 285 - hyperspectral qe,”

[91] G. Scientific, “Uprtek pg100n handheld spectrometer,”

[92] M. Panalytical, “Asd handheld 2: Hand-held vnir spectroradiometer,”

[93] A. Burkart, S. Cogliati, A. Schickling, and U. Rascher, “A novel uav-based ultra-light weight spectrometer for field spectroscopy,” *IEEE Sensors Journal*, vol. 14, pp. 62–67, Jan 2014.

[94] O. Optics, “Sts-vis,”

[95] K. D. Long, E. V. Woodbum, and B. T. Cunningham, “Design and demonstration of the transmission, reflection, and intensity (tri)-analyzer instrument for portable spectroscopy,” in *2017 IEEE Healthcare Innovations and Point of Care Technologies (HI-POCT)*, pp. 253–256, Nov 2017.

[96] L. Schmitt, "Handheld spectral analyzer turns smartphone into diagnostic tool,"

[97] K. D. Long, E. V. Woodburn, H. M. Le, U. K. Shah, S. S. Lumetta, and B. T. Cunningham, "Multimode smartphone biosensing: the transmission, reflection, and intensity spectral (tri)-analyzer," *Lab Chip*, vol. 17, pp. 3246–3257, 2017.

[98] A. A. Bodkin, A. Sheinis, A. Norton, J. Daly, S. Beaven, and J. Weinheimer, "Snapshot hyperspectral imaging: the hyperpixel array camera," vol. 7334, pp. 7334 – 7334 – 11, 2009.

[99] A. Bodkin, A. Sheinis, A. Norton, J. Daly, C. Roberts, S. Beaven, and J. Weinheimer, "Video-rate chemical identification and visualization with snapshot hyperspectral imaging," vol. 8374, pp. 8374 – 8374 – 13, 2012.

[100] C. B. Roberts, A. Bodkin, J. T. Daly, and J. Meola, "High spatial resolution lwir hyperspectral sensor," vol. 9482, pp. 9482 – 9482 – 10, 2015.

[101] Z. Zobenica, R. W. van der Heijden, M. Petruzzella, F. Pagliano, T. Xia, L. Midolo, M. Cotrufo, Y. . Cho, F. W. M. van Otten, and A. Fiore, "Integrated spectrometer and displacement sensor based on mechanically tunable photonic crystals," in *2017 International Conference on Optical MEMS and Nanophotonics (OMN)*, pp. 1–2, Aug 2017.

[102] T. Liu, F. Pagliano, and A. Fiore, "Nano-opto-electro-mechanical switch based on a four-waveguide directional coupler," *Opt. Express*, vol. 25, pp. 10166–10176, May 2017.

[103] Z. Zobenica, R. van der Heijden, M. Petruzzella, F. Pagliano, R. Leijssen, T. Xia, L. Midolo, M. Cotrufo, Y. Cho, F. Van Otten, E. Verhagen, and A. Fiore, "Integrated nano-opto-electro-mechanical sensor for spectrometry and nanometrology," *Nature Communications*, vol. 8, pp. 1–8, 12 2017.

[104] M. E. G. D. J. Brady, "Compressive imaging spectrometers using coded apertures," vol. 6246, pp. 6246 – 6246 – 9, 2006.

[105] A. Wagadarikar, R. John, R. Willett, and D. Brady, "Single disperser design for coded aperture snapshot spectral imaging," *Appl. Opt.*, vol. 47, pp. B44–B51, Apr 2008.

[106] A. A. Wagadarikar, N. P. Pitsianis, X. Sun, and D. J. Brady, "Video rate spectral imaging using a coded aperture snapshot spectral imager," *Opt. Express*, vol. 17, pp. 6368–6388, Apr 2009.

[107] A. S. Luthman, S. Dumitru, I. Quiros-Gonzalez, J. Joseph, and S. E. Bohndiek, "Fluorescence hyperspectral imaging (fhsi) using a spectrally resolved detector array," *Journal of Biophotonics*, vol. 10, no. 6-7, pp. 840–853.

[108] S. T. Neelam Gupta, Philip R. Ashe, "Miniature snapshot multispectral imager," *Optical Engineering*, vol. 50, pp. 50 – 50 – 10, 2011.

[109] E. L. Dereniak, "From the outside looking in: developing snapshot imaging spectropolarimeters," vol. 9186, pp. 9186 – 9186 – 13, 2014.

[110] K. Zidek, O. Denk, J. Hlubucek, and J. Vaclavik, "Compact and robust hyperspectral camera based on compressed sensing," vol. 10151, pp. 10151 – 10151 – 7, 2016.

[111] J. G. Dwight, T. S. Tkaczyk, D. Alexander, M. E. Pawlowski, J. C. Luvall, P. F. Tatum, and G. J. Jedlovec, "Compact snapshot image mapping spectrometer (snap-ims) for hyperspectral data cube acquisition using unmanned aerial vehicle (uav) environmental imaging," vol. 10657, pp. 10657 – 10657 – 9, 2018.

[112] S. Bish, Y. Wang, J. W. Tunnell, and X. Zhang, "Mems scanner based handheld fluorescent hyperspectral imaging system," in *2011 16th International Solid-State Sensors, Actuators and Microsystems Conference*, pp. 2542–2545, June 2011.

[113] T. Yang, X. L. Huang, H. P. Ho, C. Xu, Y. Y. Zhu, M. D. Yi, X. H. Zhou, X. A. Li, and W. Huang, "Compact spectrometer based on a frosted glass," *IEEE Photonics Technology Letters*, vol. 29, pp. 217–220, Jan 2017.

[114] J. Itatani, F. Quéré, G. L. Yudin, M. Y. Ivanov, F. Krausz, and P. B. Corkum, "Attosecond streak camera," *Phys. Rev. Lett.*, vol. 88, p. 173903, Apr 2002.

[115] M. Schultze, M. Fieß, N. Karpowicz, J. Gagnon, M. Korbman, M. Hofstetter, S. Neppl, A. L. Cavalieri, Y. Komninos, T. Mercouris, C. A. Nicolaides, R. Pazourek, S. Nagele, J. Feist, J. Burgdörfer, A. M. Azzeer, R. Ernstorfer, R. Kienberger, U. Kleineberg, E. Goulielmakis, F. Krausz, and V. S. Yakovlev, "Delay in photoemission," *Science*, vol. 328, no. 5986, pp. 1658–1662, 2010.

[116] M. Schultze and R. Kienberger, "Attosecond metrology and spectroscopy," in *Modern Metrology Concerns* (L. Cocco, ed.), ch. 12, Rijeka: IntechOpen, 2012.

[117] I. Costantini, J.-P. Ghobril, A. P. Di Giovanna, A. L. A. Mascaro, L. Silvestri, M. C. Mellenbroich, L. Onofri, V. Conti, F. Vanzi, L. Sacconi, R. Guerrini, H. Markram, G. Iannello, and F. S. Pavone, "A versatile clearing agent for multi-modal brain imaging," *Scientific Reports*, vol. 5, April 2015.

[118] L. Silvestri, M. C. Muellenbroich, I. Costantini, A. P. Di Giovanna, L. Sacconi, and F. S. Pavone, "Rapid: Real-time image-based autofocus for all wide-field optical microscopy systems," *bioRxiv*, 2017.

[119] D. Vega, K. C. Kiekens, N. C. Syson, G. Romano, T. Baker, and J. K. Barton, "Full optical model of micro-endoscope with optical coherence microscopy, multiphoton microscopy and visible capabilities," vol. 10470, pp. 10470 – 10470 – 14, 2018.

[120] P. T. S. DeVore, B. W. Buckley, M. H. Asghari, D. R. Solli, and B. Jalali, "Coherent time-stretch transform for near-field spectroscopy," *IEEE Photonics Journal*, vol. 6, pp. 1–7, April 2014.

[121] A. Mahjoubfar, D. Churkin, S. Barland, N. Broderick, S. Turitsyn, and B. Jalali, "Time stretch and its applications," *Nature Photonics*, vol. 11, pp. 341–351, 6 2017.

Appendix A Example of object detection using VNIR HSI

To demonstrate the ability of a VNIR-only hyperspectral sensor to detect camouflage and distinguish it from other plastics, we conducted an experiment at the MITRE/McLean campus. Various plastics and rocks were arrayed on the ground at the corner of the MITRE 3 parking garage and imaged looking nadir from the highest deck. The goal of the experiment was the detection of camouflage material, but the rocks were also placed because minerals as well as plastics are traditionally detected and identified with hyperspectral sensors sensitive in the SWIR and their detection with a VNIR-only sensor was under consideration.

The tests were conducted over the course of two consecutive days July 26 and July 27, 2018. The July 27 test was deliberately chosen on a partly cloudy day where illumination levels were variable. Three identical samples of camouflage material were placed in the scene on July 27, with one sample placed partially under foliage. In addition, three different rocks were emplaced. We will show our detection results obtained from dark subtracted raw data from the OKSI VNIR imaging sensor. We used the Adaptive Cosine Estimator (ACE)[66] matched filter detector using signatures collected from the images. Figure A-1 (left) shows an RGB of the tableau of July 27 from the VNIR hyperspectral imager. Figure A-1 (right) shows an iPhone photograph of a close-up of the tableau with the three rocks. The lava rock is highlighted within a red rectangle. Figures A-2 shows the detection planes of the lava rock. The left image is the result using the spectral signature derived from that same hyperspectral data cube. The right image shows the detection result when the signature of Figure A-2 (left) is used on a different hyperspectral data cube at different illumination level. More false alarms appear in the right image, but the lava rock is still detected. Figure A-3 (left) repeats the RGB image of Figure A-1 (left) for comparison to Figure A-3 (right). In Figure A-3 (right) we show the detections obtained with no false alarms of all three examples of the camouflage materials using the signature derived from a sample from the same image. In Figure A-4, we obtained weaker detections with some false alarms when using the A-3 (right) signature on an image collected 13 minutes later and under different illumination conditions.

On July 26, we placed only one example of the camouflage panel in the scene. An RGB of that tableau is shown in Figure A-5 (left). Using the same signature from July 27, we obtained the detection result of the camouflage panel shown in Figure A-5 (right). False alarms are evident in the detection image, but the panel is clearly seen.

Figure A-1: (Left)RGB from cube 2018-07-27_15_46_10 showing layout of tarps, rocks, string.(Right) Photograph of region containing lava rock.

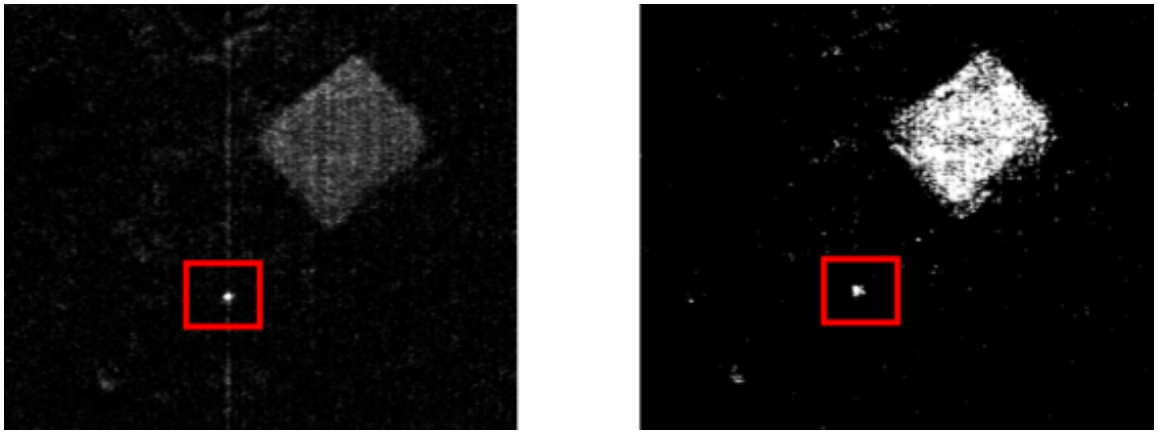

Figure A-2: (Left)Lava rock detection on cube 2018-07-27_15_46_10 using signature from same cube. (Right) Detection on cube 2018-07-27_15_37_39 using signature from different cube 2018-07-27_15_46_10. Detections is still possible, but there are many more false alarms.

Figure A-3: (Left)RGB from cube 2018-07-27_15_46_10. (Right)Camo detection on cube 2018-07-27_15_46_10 using signature from same cube.

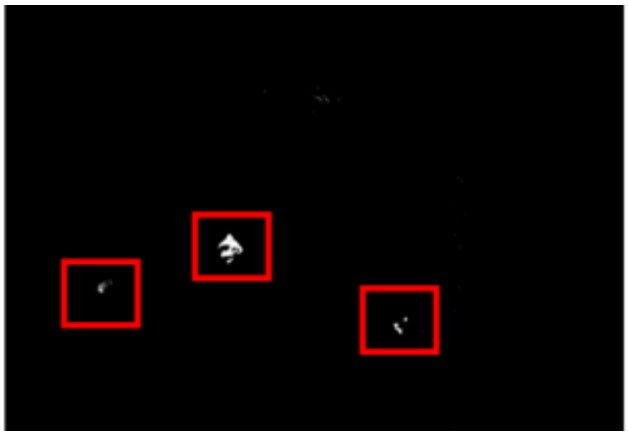

Figure A-4: Detection on cube 2018-07-27_15_33-11 using signature from different cube 2018-07-27_15_46_10. Detections is still possible, but there are more false alarms.

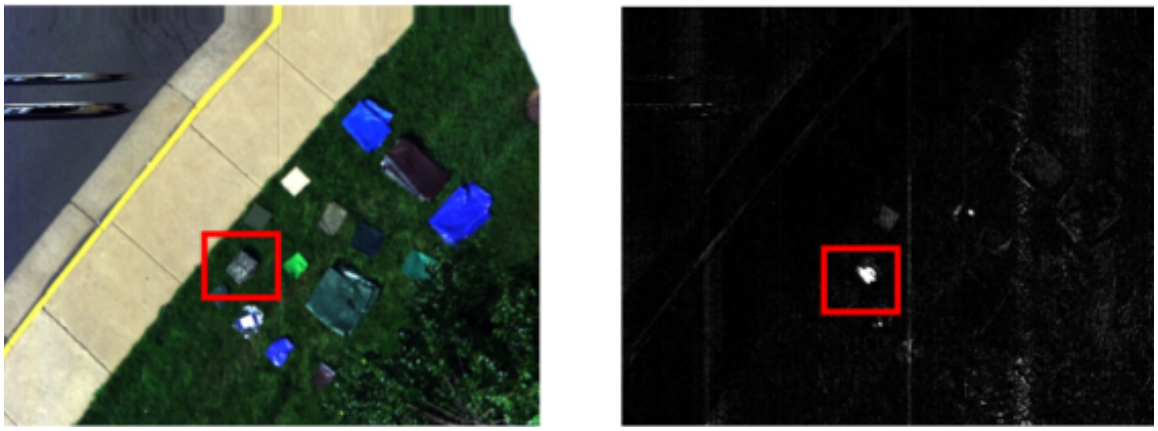

Figure A-5: (Left) RGB from cube 2018-07-26_21_19_03. (Right) Camo detection on cube 2018-07-26_21_19_03 using signature from different cube 2018-07-27_15_46_10.

This page intentionally left blank.

Appendix B Table of Vendors and their products

The following tables provide the reader with a quick reference to the commercial hyperspectral imaging systems that were mentioned in the write-up above and the scientific ones that did not make it into the paper. Populating the cost field of the commercial systems table was the primary driver for its creation. However, if no cost exists for a system, it is because the vendor did not respond within the limited timeframe the data was compiled.

The scientific systems table provides the technologies that were researched but did not fit into the definition of a commercial snapshot imaging spectrometer. However, defining state-of-the-art is a moving target, and as such getting a handle on what is currently being researched is a good indicator of what is to come down the line. The table lists the various research efforts by an informal - sometimes generic - name as specified by the creator of the tables and the associated group involved in that work. Due to limited space, typically only the first author of the published work was listed in the group field.

Table B-1: Commerical Hyperspectral Imaging Systems

Filter Type	Arch.	Sensor	Pixel Pitch [μm]	Spatial Res. [px]	Spectral			Acq. Rate [$frames/sec$]	Cost [$]	MFR	Refs
					Range [nm]	# Bands	Res. [nm]				
4x4 Mosaic**,1	DoFP[2]	CMOS	5.5	512 x 272	470-630	16	10	170 [$cubes/sec$]	17,500	Ximea[3]	[67]
5x5 Mosaic	DoFP	CMOS	5.5	409 x 217	600-975	25	15	170 [$cubes/sec$]	17,500	Ximea	[68]
Wedge[4]	DoFP	CMOS	5.5	2048 x 5	470-900	150	3	850 [ln/sec]	23,000	Ximea	[69]
Wedge	DoFP	CMOS	5.5	2048 x 8	600-975	100	4	1360 [ln/sec]	17,500	Ximea	[70]
Pushbroom	Scanner[5]	CMOS	17.58	512 x 512	400-1000	204[6]	7	0.6-300[7] [sec]	19,950	Specim	[71]
Dichroic[8]	DoFP	CCD	7.4	2&4MP	400-1000	4 OR 6[9]	-	15	-	Pixelteq	[72]
Dichroic	DoFP	InGaAs	25	640 x 512	700-1700	4 OR 3[10]	-	30	-	Pixelteq	-
-	Scanner	-	-	-	400-750	35	10	10	439	AlphaNOV	[73]
-	-[11]	-	-	-	450-1000	-	-	-	550-4,000	Stratio Inc.	[74]
-	-	-	-	-	800-1200	-	-	-	-	Stratio Inc.	-
4x4 Mosaic**	DoFP	CMOS	5.5	512 x 272	470-630	16	10	50	11,540	PhotonFocus	[75]
5x5 Mosaic	DoFP	CMOS	5.5	409 x 218	600-975	25	15	50	11,540	PhotonFocus	[76]
Wedge	DoFP	CMOS	5.5	2048 x 5	470-900	150	3	42	11,807	PhotonFocus	[77]
Wedge	DoFP	CMOS	5.5	2048 x 8	600-975	100	4	42	11,540	PhotonFocus	[78]
-	DoFP	-	-	200 x 400	600-1000	20-25	12	8	18,980	BaySpec	[79–81]
4x4 Mosaic**	DoFP	CMOS	5.5	512 x 272	470-620	16	10	-	12,500	3DOne	[82]
5x5 Mosaic	DoFP	CMOS	5.5	409 x 218	600-975	25	15	-	12,500	3DOne	-
Wedge	DoFP	CMOS	5.5	2048 x 5	470-975	150	3	-	15,000	3DOne	-
-[12]	Scanner	-	-	-	400-1000	550	4	2 [sec]	18,000	TruTag	[83]

** All of the Mosaic & Wedge type filters in the table are from IMEC hyperspectral sensors.

1. Mosaic type filters are usually associated with snapshot systems.
2. Division of Focal Plane (DoFP)[6].
3. Ximea also offers board-level versions of their HSI cameras.
4. Wedge type filters are usually associated with linescane systems.
5. Measurement of target area is made in a pushbroom fashion (i.e. linescan mode with an integrated scanner)[22].
6. Binning at 2x: 102 & binning at 3x: 68 spectral bands.
7. Dependent upon illumination level.
8. Pixelteq in-house patented technology [23].
9. RGB + NIR or RGB + 3xNIR.
10. NIR + SWIR.
11. The following references were published pre-LinkSquare during the R&D phase [28, 84, 85].
12. Off-sensor spectral filtering, bypassing spatial/spectral tradeoff.

Table B-2: Commerical Hyperspectral Imaging Systems Cont'd

Filter Type	Arch.	Sensor	Pixel Pitch [μm]	Spatial Res. [px]	Spectral			Acq. Rate [$frames/sec$]	Cost [$]	MFR	Refs
					Range [nm]	# Bands	Res. [nm]				
-	Scanner[1]	CMOS	12.5	256 x 1	340-780	29	15	5-10 [sec]	245	Hamamatsu	[86]
-**	DoFP	CMOS	5.5	2040 x 2046[2]	-	-	-	180	-	Tattile	[87]
-	DoFP	CCD	-	-	450-950	125	8	5 [$cubes/sec$]	40,000	Cubert	[88]
-	DoFP	CCD	-	-	-[3]	125	10	15 [$cubes/sec$]	50,000	Cubert	[89]
-	DoFP	CCD	-	-	450-950	125	8	20 [$cubes/sec$]	35,000	Cubert[4]	[90]
-	Scanner	CCD	-	-	380-780	-	-	0.002-2 [sec]	2,489	Gamma Sci.	[91]
-	Scanner	-	-	-	325-1075	-	3	0.0085 [sec]	13,000-25,000	Malvern Panalytical	[92]
-	Scanner	CMOS	7.8	1024 x 1	350-800[5]	-	3	10μ-10 [sec]	1,500	Ocean Optics	[93, 94]

1. This is a secondary product that was meant to be integrated with other devices.
2. The spatial resolution reported is without any spectral considerations.
3. Options: 355-750, 450-950, 550-1000.
4. There is an underwater version of this device available as well.
5. Additional spectral ranges available: UV (190-650) & NIR (650-1100).

Table B-3: Scientific Hyperspectral Imaging Systems

Name	Arch.	Sensor	Spectral			Acq. Rate [$frames/sec$]	Cost [$]	Group	Refs
			Range [nm]	# Bands	Res. [nm]				
TRI-Analyzer	[95]	-	VIS	-	-	5-20	550	UIS-UC	[96, 97]
Hyperpixel Array Camera	Snapshot	CCD	-[1]	-	-	15 [$cubes/sec$]	-	Bodkin D&E	[98–100]
Nano-opto-electro-mechanical sensor	Scanner	-	-	-	0.08	-	-	TUe	[101–103]
Coded Aperture Snapshot Spectral Imager	Snapshot	-	-	-	-	-	-	Duke et. el.	[104–106]
Image Mapping Spectroscopy Endoscope	Snapshot	CCD	450-650	48	4-10	5.2	-	Rice Univ.	[44]
Image Mapping Spectrometer	Snapshot	CCD	450-650	24	8	10 [sec]	-	Rice Univ.	[45]
MEMS Fabry-Perot Interferometer	Scanner	-	4200-4400	8	60-80	$<$ 30 [sec]	-	VTT	[34, 36]
Imaging Spectrometer	Snapshot	-	450-700	50	-	3 [msec]	-	JPL	[40]
Retinal Camera	Snapshot	-	470-650	48	-	5.2	-	Rice & Columbia	[41]
Spectral Resolving Detector Array	Snapshot	-	460-630	16	-	20	-	Northwestern	[42]
Hemodynamic Response Imager	Snapshot	CMOS	481-632	16	15	20-30	-	Poly. Mon. et. el.	[47]
Macular Degen. Imaging Spectrometer	Snapshot	-	-	-	-	-	-	NEI et. el.	[43]
Imaging Spectrometer	Snapshot	CMOS	480-660	60	-	12 [sec]	-	Vanderbilt & Rice	[46]
Fluorescence HSI	Pushbroom	CMOS	600-1000	100	-	0.01 [sec]	-	Cambridge	[107]
Miniature Multispectral Imager	Snapshot	InGaAs	1487-1769	10	-	-	-	U.S. ARL	[108]
Spectro-Polarimeter	Snapshot	CCD	400-760	31	-	30 [msec]	-	UofA.	[109]
Coded Aperture Snapshot Spectral Imager	Snapshot	CMOS	-	-	-	-	-	TOPTEC et. al.	[110]
SNAP-IMS	Snapshot	CCD	470-670	55	-	2-10 [msec]	-	Rice et. al.	[111]
MEMS HSI	Scanner	CMOS	490-730	15	20	1	-	UTAustin	[112]
Frosted Glass Spectrometer	Snapshot	CCD	400-800	-	4.25	-	-	-	[113]
Attosecond Spectroscopy	-	-	380-480	-	-	-	-	Max Planck Inst.	[114–116]
Neuro & Cardiac Imaging	Scanner	-	-	-	-	-	-	LENS	[117, 118]
OCM	MPM	-	-	-	-	-	-	UofA	[119]
Time Stretch Fourier Transform	-	-	-	-	-	-	-	UCLA et. al.	[120, 121]

** These systems are considered active research.

1. VNIR, MWIR, and LWIR version.